# Site-specific analysis of heteronuclear Overhauser effects in microcrystalline proteins

**ARTICLE** *in* JOURNAL OF BIOMOLECULAR NMR · JULY 2014

Impact Factor: 3.14 · DOI: 10.1007/s10858-014-9843-1 · Source: PubMed



**10 AUTHORS**, INCLUDING:

Riddhiman Sarkar
Technische Universität München
**27** PUBLICATIONS **624** CITATIONS
SEE PROFILE

Sam Asami
Technische Universität München
**10** PUBLICATIONS **152** CITATIONS
SEE PROFILE

Oliver F Lange
Technische Universität München
**43** PUBLICATIONS **2,821** CITATIONS
SEE PROFILE

Bernd Reif
Technische Universität München
**124** PUBLICATIONS **4,212** CITATIONS
SEE PROFILE

J Biomol NMR (2014) 59:241–249
DOI 10.1007/s10858-014-9843-1

ARTICLE

# Site-specific analysis of heteronuclear Overhauser effects in microcrystalline proteins

**Juan Miguel Lopez del Amo · Vipin Agarwal · Riddhiman Sarkar · Justin Porter · Sam Asami · Martin Rübbelke · Uwe Fink · Yi Xue · Oliver F. Lange · Bernd Reif**

Received: 7 April 2014 / Accepted: 20 June 2014 / Published online: 3 July 2014


**Abstract** Relaxation parameters such as longitudinal relaxation are susceptible to artifacts such as spin diffusion, and can be affected by paramagnetic impurities as e.g. oxygen, which make a quantitative interpretation difficult. We present here the site-specific measurement of $[^1H]^{13}C$ and $[^1H]^{15}N$ heteronuclear rates in an immobilized protein. For methyls, a strong effect is expected due to the three-fold rotation of the methyl group. Quantification of the $[^1H]^{13}C$ heteronuclear NOE in combination with $^{13}C$-$R_1$ can yield a more accurate analysis of side chain motional parameters. The observation of significant $[^1H]^{15}N$ heteronuclear NOEs for certain backbone amides, as well as for specific asparagine/glutamine sidechain amides is consistent with MD simulations. The measurement of site-specific heteronuclear NOEs is enabled by the use of highly deuterated microcrystalline protein samples in which spin diffusion is reduced in comparison to protonated samples.

**Keywords** MAS solid-state NMR · Deuteration · Protein dynamics · Spin relaxation

## Introduction

Nuclear relaxation is a consequence of molecular motion resulting from reorientation of the dipole and CSA interactions with respect to the external magnetic field. As such, it is an intrinsic feature of solution-state NMR. Also in the solid-state, local dynamics yield fluctuations of magnetic fields, resulting in nuclear relaxation. In the past, longitudinal (Cole and Torchia 1991; Giraud et al. 2004; Chevelkov et al. 2008),

Juan Miguel Lopez del Amo and Vipin Agarwal have contributed equally to this work.

J. M. L. d. Amo · R. Sarkar · J. Porter · S. Asami · M. Rübbelke · O. F. Lange · B. Reif (✉)
Munich Center for Integrated Protein Science (CIPS-M) at Department Chemie, Technische Universität München (TUM), Lichtenbergstr. 4, 85747 Garching, Germany
e-mail: reif@tum.de

J. M. L. d. Amo · R. Sarkar · J. Porter · S. Asami · M. Rübbelke · O. F. Lange · B. Reif
Helmholtz-Zentrum München (HMGU), Deutsches Forschungszentrum für Gesundheit und Umwelt, Ingolstädter Landstr. 1, 85764 Neuherberg, Germany

J. M. L. d. Amo · V. Agarwal · U. Fink · B. Reif
Leibniz-Institut für Molekulare Pharmakologie (FMP), Robert-Rössle-Str. 10, 13125 Berlin, Germany

*Present Address:*
J. M. L. d. Amo
CIC Energigne, Albert Einstein 48, 0150 Miñano, Spain

*Present Address:*
V. Agarwal
ETH Zurich, Wolfgang-Pauli-Str. 10, 8093 Zuerich, Switzerland

Y. Xue
Department of Chemistry, Purdue University, West Lafayette, IN 47907-2084, USA

*Present Address:*
Y. Xue
Department of Biochemistry, Duke University Medical Center, Durham, NC 27710, USA

cross-correlated relaxation rates (Chevelkov et al. 2007a, b; Linser et al. 2010), as well as order parameters (Lorieau and McDermott 2006; Chevelkov et al. 2009a; Hou et al. 2011; Schanda et al. 2011) have been measured for uniformly isotopically enriched, immobilized biomolecules. This has enabled the quantification of backbone and side chain dynamics (Chevelkov et al. 2009b; Schanda et al. 2010; Knight et al. 2012). The data was analyzed within the framework of the extended model-free theory, and showed the presence of small-amplitude motions with slow motional correlation times in the range of 5 and 150 ns. Additionally, information on slow µs–ms timescale motion has been obtained from $R_{1\rho}$ experiments (Helmus et al. 2008; Krushelnitsky et al. 2010; Lewandowski et al. 2011b; Byeon et al. 2012; Quinn and McDermott 2012; Zinkevich et al. 2013) or CPMG (Tollinger et al. 2012). In the solid-state, observables such as spin–lattice relaxation rates are dependent on other parameters such as the nuclear spin density or the concentration of paramagnetic impurities as e.g. dissolved oxygen. Furthermore, the longitudinal relaxation rate $R_1$ is MAS dependent and can be affected by spin-diffusion (Fry et al. 2011). This makes an absolute quantitative interpretation of the experimental rate rather difficult. Other observables such as the dipole-CSA cross-correlated relaxation rate $\eta$ and $R_{1\rho}$ do not require such calibration. E.g. $\eta$ is exclusively sensitive to slow dynamics with correlation times larger than 1 ns.

We present here the first quantification of site-specific heteronuclear $^{13}C[^1H]$ and $^{15}N[^1H]$ Overhauser enhancements in a microcrystalline protein sample. The heteronuclear NOE is sensitive to motion on a sub-ns timescale and therefore allows to unambiguously identify dynamics with motional correlation times in the picosecond regime. Heteronuclear NOE experiments in the solid-state have been pioneered by Gibby, Pines and Waugh (Gibby et al. 1972) and applied to small molecules by Haw, Law and coworkers (White and Haw 1990; Higgins et al. 2002). Takegoshi and Terao suggested to exploit the heteronuclear NOE expected for methyl groups for polarization transfer instead of cross-polarization (Takegoshi and Terao 2002). This has subsequently been applied to proteins (Katoh et al. 2004; Purusottam et al. 2013). The first assessment of protein dynamics by interpretation of heteronuclear NOE experiments in the solid-state was reported by Emsley and co-workers (Giraud et al. 2006). In their work, non-specific heteronuclear NOEs between water and the bulk amide backbone have been observed, and potential magnetization pathways are discussed. We show here that heteronuclear NOEs can be quantified in the solid-state with site-specific resolution. The experiments are carried out using a perdeuterated sample of the chicken α-spectrin SH3 domain. We believe that quantification of heteronuclear NOEs will be important for model-free analyses involving two independent motional timescales, requiring at least four linear independent observables.

## Results and discussion

In the past, we and others proposed a labelling scheme that is based on extensive deuteration to eliminate undesired proton–proton dipolar interactions (Chevelkov et al. 2006; Schanda et al. 2009; Akbey et al. 2010; Knight et al. 2011). The perdeuterated protein is recrystallized from a buffer containing $D_2O$ in order to suppress anisotropic interactions among exchangeable sites. This results in significant narrowing of the proton resonance, yielding $^1H$ line width on the order of 20–40 Hz without application of homonuclear decoupling. The amount of $D_2O$ required in the crystallization buffer depends on the experimental MAS rotation frequency (Akbey et al. 2010; Lewandowski et al. 2011a). Given the fact that high power heteronuclear and homonuclear decoupling is not required, sample heating is avoided and dynamic properties can be quantified with high accuracy (Linser et al. 2007).

Initially, we performed $[^1H]^{13}C$ heteronuclear NOE experiments. For methyl groups, a significant heteronuclear NOE effect is expected due to the fast three-fold rotation of the $CH_3$ group. For these experiments, a sample was employed in which the growth medium was supplemented with specifically labeled α-ketoisovalerate to yield selective enrichment of valines and leucines methyl groups ($^{13}C^1H^2D_2$) (Agarwal et al. 2008). Similar spectra are observed for uniformly $^2H$ and $^{13}C$ isotopically enriched samples, exploiting the fact that the chemicals which are used as nutrients in the bacterial growth medium have an isotopic purity on the order of 97 % (Agarwal and Reif 2008). This allows to detect methyl group protons with high sensitivity and resolution.

A HOESY experiment was recorded using the pulse scheme in Fig. 5a. The corresponding spectrum is represented in Fig. 1a. Peak intensities for the heteronuclear NOE are not uniform and vary significantly for different methyl groups. We observe additional cross peaks that represent correlations between specific carbon resonances and two or more proton resonances. These additional cross peaks are presumably due to $^1H,^1H$ spin diffusion. In fact, the methyl groups of V9, V44 and V53 are located in the hydrophobic core of the protein and are all within a distance of 4–5 Å. In principle, RAP labeling (Asami et al. 2010) in combination with fast spinning (Asami and Reif 2013) can yield a more efficient dilution of the protein spin system to overcome this issue.

Quantitative heteronuclear NOEs enhancement factors were obtained by comparing $^1H,^{13}C$ cross peak intensities of spectra that were recorded with on- and off-resonance

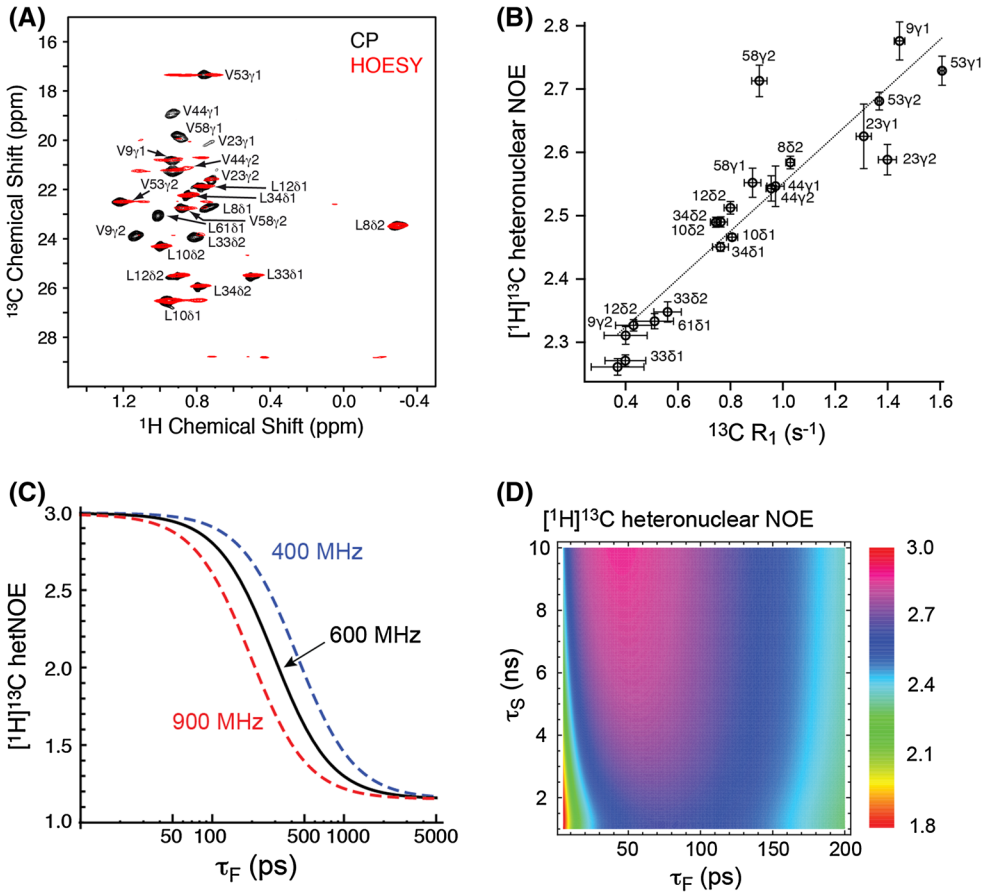


**Fig. 1** **a** $^{1}$H,$^{13}$C correlation spectra obtained using CP (*black*) and heteronuclear NOE (pulse scheme in Fig. 5a). For clarity, the axes of the hetNOE experiment have been swapped. The NOE mixing time was set to 150 ms. The experiment was recorded using a perdeuterated SH3 sample which was selectively protonated in leucine and valine residues (Agarwal et al. 2008). **b** Correlation between the experimental heteronuclear NOE enhancement and the $^{13}$C $R_1$ relaxation rate using the experimental scheme depicted in Fig. 5b. The carbon longitudinal relaxation data are taken from (Agarwal et al. 2008). **c** Theoretical [$^{1}$H]$^{13}$C heteronuclear NOE rates within the framework of a model-free analysis, for magnetic field strengths of 9.4 T (400 MHz, *blue*), 14.1 T (600 MHz, *black*) and 21.1 T (900 MHz, *red*). In the simulation, $S_F^2 = 0.6$ has been assumed. **d** [$^{1}$H]$^{13}$C heteronuclear NOE rates as a function of the motional correlation times $\tau_S$ and $\tau_F$ in the framework of an extended model-free analysis. In the simulation, the order parameters are set to $S_F^2 = 0.6$ which is a typical values found for Val and Leu side chain methyl groups (Ishima et al. 2001b; Skrynnikov et al. 2002). It is found that the slow motional order parameter $S_S^2$ has a small influence on the magnitude of the heteronuclear NOE. In the simulation, $S_S^2$ was set to 0.6

proton irradition prior to the $^{13}$C excitation pulse (pulse scheme in Fig. 5b). In the steady-state, the heteronuclear NOE is given by the equation (Cavanagh et al. 1996)

$$\text{hetNOE} = 1 + \frac{\gamma_H}{\gamma_C} \cdot \frac{R(hetNOE)}{R(C_z)} \quad (1)$$

$R(C_z)$ and $R(hetNOE)$ refer to the carbon longitudinal relaxation rate and the heteronuclear NOE rate, respectively, which can be quantitatively described as (Ishima et al. 2001a)

$$R(hetNOE) = c_{CH}^2[-J(\omega_H - \omega_C) + 6J(\omega_H + \omega_C)] \quad (2)$$

$$\begin{aligned} R(C_z) = {} & c_{CH}^2[J(\omega_H - \omega_C) + 3J(\omega_C) + 6J(\omega_H + \omega_C)] \\ & + 2c_{CD}^2[J(\omega_D - \omega_C) + 3J(\omega_C) + 6J(\omega_D + \omega_C)] \\ & + \delta_C^2 J(\omega_C) \end{aligned} \quad (3)$$

with $c_{CH} = (\mu_0/4\pi)\gamma_H\gamma_C\hbar/r_{CH}^3$ and $c_{CD} = (\mu_0/4\pi)(8/3)^{1/2}\gamma^D\gamma_C\hbar/r_{CD}^3$, assuming $r_{CH} = 1.115$ Å and $r_{CD} = 1.110$ Å. $\delta_C$ refers to the chemical shift anisotropy of the methyl carbon and was set to 25 ppm (Ishima et al. 2001b; Wylie et al. 2005). The model-free spectral density functions $J(\omega)$ are defined as (Agarwal et al. 2008)

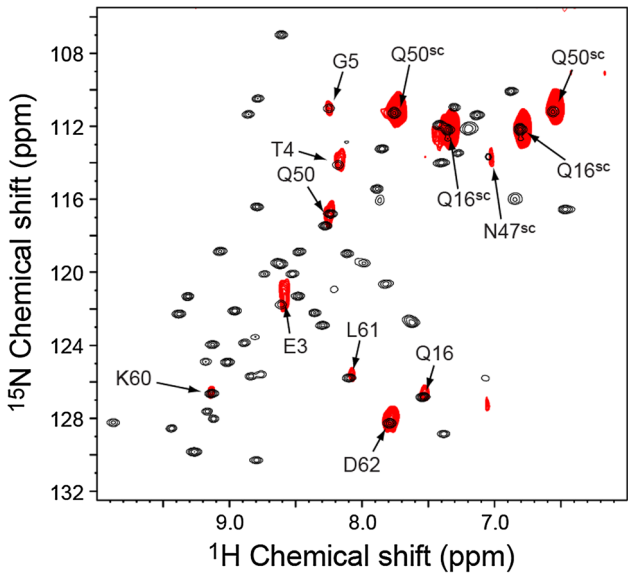


**Fig. 2** [$^{1}$H]$^{15}$N heteronuclear NOE correlation spectra (*red contours*), employing the pulse scheme represented in Fig. 5c (chemical shift evolution in $f_2$, $f_3$). The mixing time was set to 2.0 s. The reference spectrum which was recorded using INEPT for magnetization transfer is represented in *black*

$$J(\omega) = \left(1 - \frac{1}{9}S_F^2\right)\frac{\tau_F}{1+\omega^2\tau_F^2} \tag{4}$$

$S_F$ refers to the fast motion order parameter which contains fast torsional angle fluctuations in the side chain. The extended model-free spectral density function adapted to methyl groups is defined as (Clore et al. 1990)

$$J(\omega) = \left(1 - \frac{1}{9}S_F^2\right)\frac{\tau_F}{1+\omega^2\tau_F^2} + \frac{S_F^2}{9}\left(1 - S_S^2\right)\frac{\tau_S}{1+\omega^2\tau_S^2} \tag{5}$$

As the influence of the order parameter on the spectral density function is scaled due to the three-fold rotation of the methyl group, $S_F^2$ has a relatively small influence on the heteronuclear NOE. Typical values for Val and Leu side chains at room temperature are $S_F^2 = 0.6$ (Ishima et al. 2001b; Skrynnikov et al. 2002).

We find that $^{13}$C $R_1$ relaxation rates and heteronuclear NOE are highly correlated (Fig. 1b). At first sight this seems surprising, as it is found that methyl group dynamics occurs in the picosecond regime with correlation times in the range of 5–100 ps (Xue et al. 2007). For motion on this timescale, no variations of the heteronuclear NOE are expected within the framework of a model-free analysis (Fig. 1c). Inclusion of a second set of parameters ($S_S^2$, $\tau_S$), assuming the order parameter $S_S^2$ to be on the order of 0.6, and $\tau_S$ in the range of 1–3 ns yields a consistent fit for $^{13}$C-$R_1$ and the heteronuclear NOE enhancement factors.

Subsequently, we applied the approach to nitrogens to obtain dynamic information for the protein backbone and the side chain amides. Figure 2 shows a $^{1}$H,$^{15}$N correlation spectrum resulting from the 2D version of the pulse scheme represented in Fig. 5c ($f_2$, $f_3$), using a mixing time of 2.0 s for the heteronuclear NOE transfer. We find the strongest correlation peaks for the side chain amides of Q16 and Q50. Weaker transfers are observed for the N- and

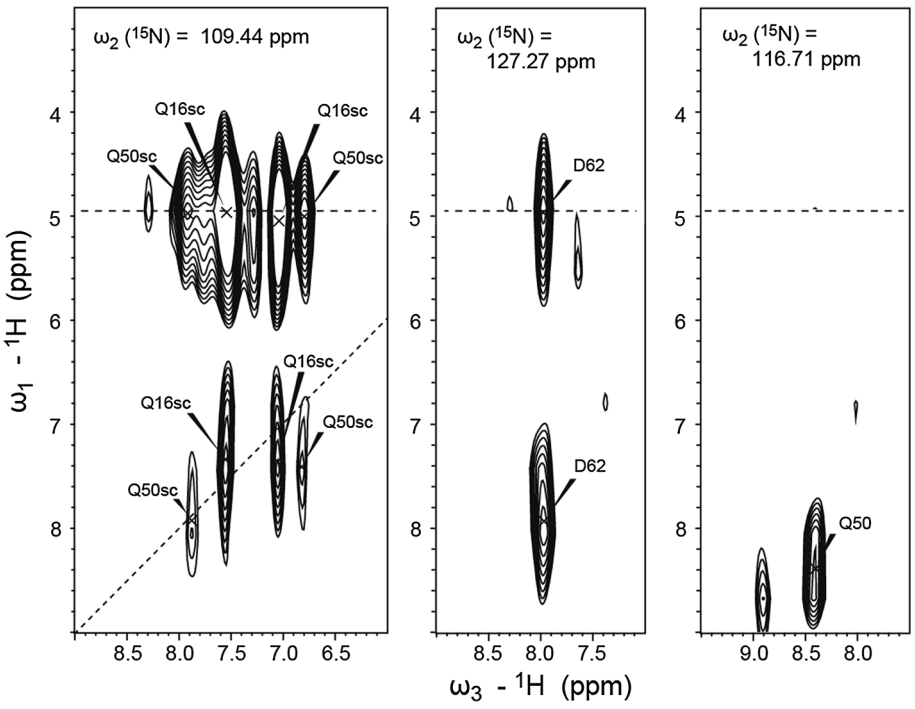


**Fig. 3** 2D-$^{1}$H, $^{1}$H planes ($f_1$,$f_3$) from the $^{1}$H detected 3D H-NH experiment using [$^{1}$H]$^{15}$N heteronuclear NOE for magnetization transfer. For the experiment, the pulse scheme represented in Fig. 5c was employed. 2D slices were selected at specific $^{15}$N chemical shifts. The hetNOE mixing time was set to 500 ms

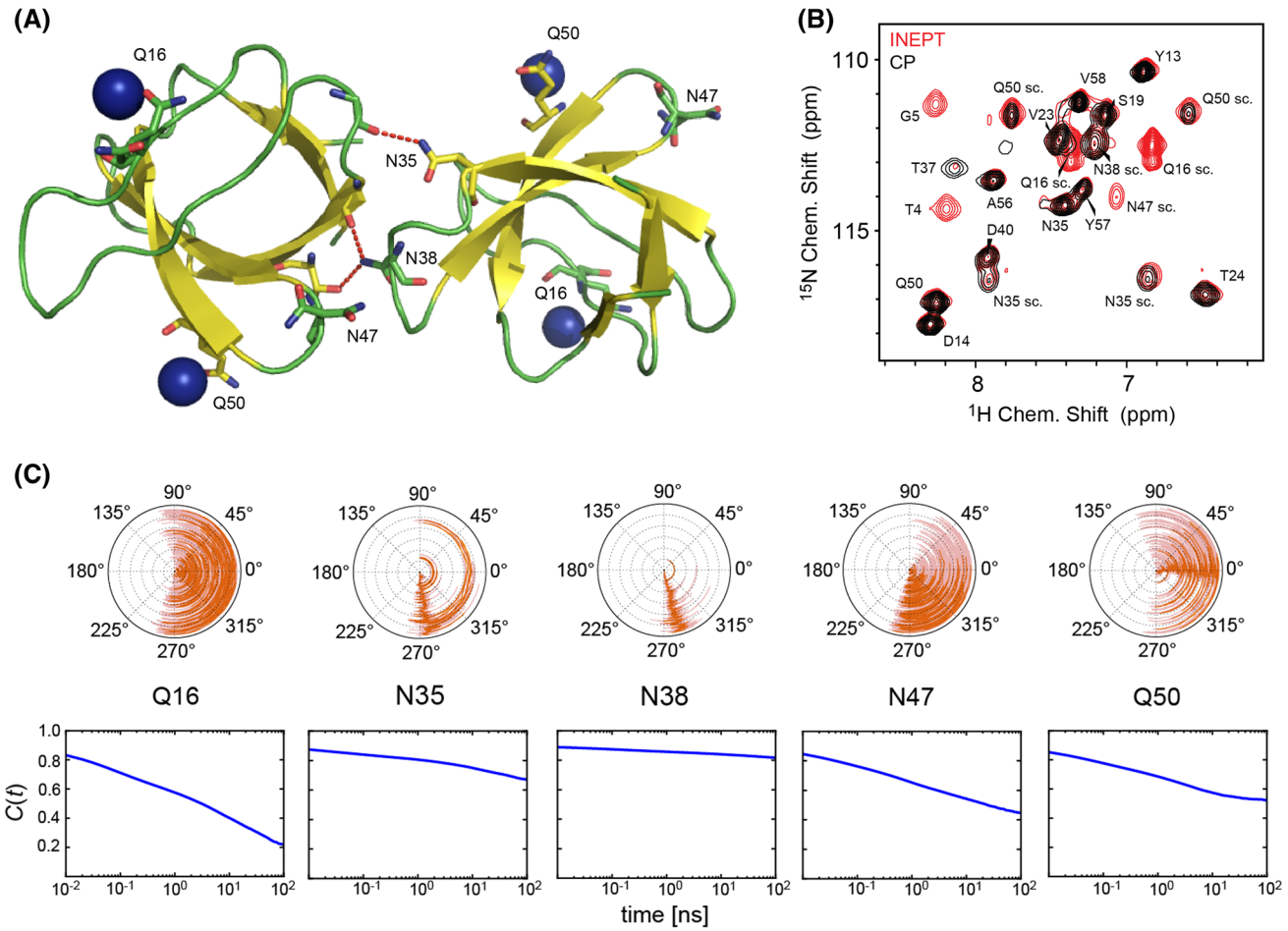


**Fig. 4** **a** Structural model of the α-spectrin SH3 domain (PDB ID: 1U06). The protein adopts a dimeric structure in the crystal unit cell. Solvent accessibility is indicated by water spheres. **b** $^{1}H,^{15}N$ correlation spectrum of the α-spectrin SH3 domain using INEPT (*red contours*) and CP (*black contours*) for magnetization transfer. Amides which are mobile on a timescale shorter than the rotor period are not visible in the CP based experiment. **c** *Top* MD trajectory for asparagine $\chi_2$ (N35, N38 and N47), as well as glutamine $\chi_3$ (Q16 and Q50). The origin of the *circle* represents $t = 0$. Subsequent time steps are represented as $t \bullet e^{-i\chi}$, with $t$ being the radius of the circle. *Bottom* correlation functions $C(t)$ for asparagine and glutamine side chain motion, calculated from the MD trajectory

C-termini of the protein (E3, T4, G5, as well as for K60, L61 and D62).

To address the question on the origin of polarization, we recorded a 3D experiment with a $^{1}H$ chemical shift evolution period before the heteronuclear NOE mixing element (pulse scheme in Fig. 5c). We find that for the side chain amides of Q16 and Q50, magnetization originates primarily from water protons (Fig. 3). Additionally, direct correlations between side chain amide protons and nitrogens are observed. In principle, $H^N$,$H^N$ cross peaks should be aligned along the diagonal in the spectrum. However, rotation around $\chi_4$ results in chemical exchange between e.g. Q50(E)-Hδ and Q50(Z)-Hδ which yields additional cross peaks above and below the diagonal. These exchange mediated cross peaks are apparently not resolved within the spectral resolution obtained in this experiment. For D62, magnetization originates in equal parts from water and from the backbone amide proton, whereas for the backbone amide Q50, magnetization is exclusively originating from the amide proton. A correlation peak to water is absent. In MD simulations, the backbone amide of Q50 shows a high order parameter. We therefore speculate that the Q50 backbone correlation peak in Fig. 2 is caused by proton driven spin diffusion. Similarly, the backbone cross peak for Q16 might be explained. Observation of spin diffusion mediated cross peaks between side chain and backbone amides is surprising as spin diffusion should be largely suppressed by the employed deuteration scheme. Nevertheless, the extensively long mixing times of up to several seconds might faciliate the observed magnetization transfer.

Heteronuclear NOEs involving water is presumably due to indirect transfers involving the side chain amide proton as a relay nucleus.

PRE experiments show that Q16 and Q50 are both solvent accessible (Linser et al. 2009). None of the two residues is

involved in a hydrogen bond (Fig. 4a). In the X-ray structure, a water molecule is found in close vicinity of those residues (PDB ID: 1U06). By contrast, residues N35 and N38 are involved in hydrogen bonds to a SH3 molecule located in a symmetry related crystal unit cell. Water-amide spin diffusion experiments indicate that a water molecule is nearby for these two residues (Chevelkov et al. 2005). The presence of a water molecule is confirmed by a well defined electron density in the X-ray structure. However, no heteronuclear NOE can be observed indicating that the residence time for these water molecules must be much longer. Asparagine and glutamine side chains can undergo motion on a sub-nanosecond timescale. Rotations around the nitrogen Nδ/Nε carbonyl Cγ/Cδ axis are very slow due to the partial double bond character, resulting in distinct chemical shifts for the $NH_\gamma$ and $NH_\delta$ side chain amide protons, respectively. Nevertheless, the side chain can be mobile. In the α-spectrin SH3 domain, Q16 and Q50 are particularly dynamic. In the x-ray structure, the occupancies for Q16Nε, N35Nδ, N38Nδ, N47Nδ and Q50Nε are 0.4, 1.0, 1.0, 0.5, 0.8, respectively (PDB ID: 2NUZ) (Chevelkov et al. 2007b). This is consistent with MD simulations, which yield rapidly decaying correlation functions with a small overall order parameter (Fig. 4c) (Chevelkov et al. 2010). The initial decay of the correlation function is equally fast for all asparagine and side chain amide groups. Apparently, the observation of a heteronuclear NOE is only coupled to the order parameter of the motion. Whereas the motional amplitude for N35 and N38 is too small to yield a significant hetNOE, the side chains of Q16, N47 and Q50 show large enough motion to induce a significant relaxation based magnetization transfer. Fast dynamics with large amplitudes is consistent with $^1H$,$^{15}N$ correlation spectra recorded with INEPT and CP for magnetization transfer (Fig. 4b). For Q16, N47 and to a somewhat less extent for Q50, CP efficiency is reduced in comparison to INEPT type transfers indicating fast motion (Linser et al. 2010). Interestingly, a heteronuclear NOE is also observed for the amides of residues E3, T4, G5 and D62 which have been shown to undergo slow dynamics in the 10–100 ns regime recently (Chevelkov et al. 2009b; Linser et al. 2010), indicating that motion occurs on multiple timescales. Amides for which we observed previously large H/D exchange rates (primarily R21, N35sc, S36, N38sc, W41ε) (Lopez del Amo et al. 2010) do not show a significant heteronuclear NOE, indicating that fast H/D exchange is not necessarily coupled with fast dynamics.

In the future, the measurement of heteronuclear NOEs might be transferred to other than methyl groups in aliphatic side chains which are accessible via the RAP labeling scheme (Asami et al. 2010, 2012), and will allow to quantify the timescale of side chain motional processes.

## Methods

### Sample preparation

A $^2H$,$^{13}C$,$^{15}N$ labelled sample of the SH3 domain of chicken α-spectrin was produced by recombinant protein expression. The protein was purified and micro-crystallized as described previously (Chevelkov et al. 2006). Protons were partially back-exchanged at labile positions by precipitating the protein in a buffer containing 10 % $H_2O$. This proton concentration was found to be the best compromise between sensitivity and resolution at this rotation frequency (Akbey et al. 2010). Micro-crystals were

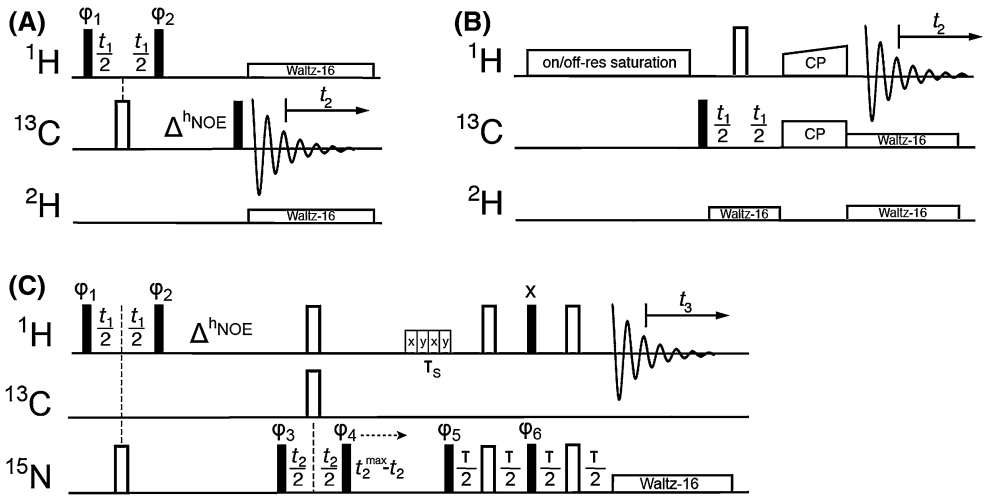


**Fig. 5** Pulse schemes employed in this study. [$^1H$]$^{13}C$ (A,B) and [$^1H$]$^{15}N$ (C) heteronuclear NOE experiments. **a** The heteronuclear detection version, whereas **b** and **c** refer to the proton detected version of the experiment. In **c**, MISSISSIPPI solvent suppression was employed prior to detection (Zhou and Rienstra 2008). The delay τ is set to 1/(2*J*), assuming an effective coupling of 92.5 and 88 Hz for the first and second INEPT step

obtained via a pH-shift from 3.5 to 7.5 overnight. The crystals were spun into a 3.2 mm rotor using approximately 15 mg protein per sample.

## NMR spectroscopy

Experiments to identify and characterize the heteronuclear NOE are represented in Fig. 5. $[^1H]^{13}C$ heteronuclear NOE experiments are shown in Fig. 5a, b, $[^1H]^{15}N$ heteronuclear NOE experiments are recorded employing the pulse schemes shown in Fig. 5c.

For proof-of-principle, a $^{13}C$ detected 2D hetNOE experiment was recorded, accumulating 192 increments in the indirect $^1H$ evolution period ($t_1^{max} = 25$ ms) with 512 scans each (pulse scheme in Fig. 5a). A spin-temperature filter is implemented to ensure that magnetization originates from protons ($\varphi_1 = +x, -x$; $\varphi_1 = 2(+x), 2(-x)$; $\varphi_{REC} = +x, -x, -x, +x$). The recycle delay was set to 1.6 s, and the experimental time for this experiment amounted to 44 h.

An increase in sensitivity is achieved using proton detected experiments (Fig. 5b). Quantitative values for $[^1H]^{13}C$ heteronuclear NOE enhancements are obtained by comparing spectra with on- and off resonance saturation for 80 and 600 ms. Proton saturation pulses were applied with alternating x and y phases. The employed rf field on the $^1H$ channel was set to 8 kHz. In the quantitative het-NOE experiments, 80 increments ($t_1^{max} = 20$ ms) with 128 scans each were accumulated (recycle delay = 8.0 s) to yield a total experimental time of ca. 24 h.

The $[^1H]^{15}N$ heteronuclear NOE is implemented using a longitudinal mixing time during which magnetization is allowed to exchange from the proton to the heteronuclear spin (Fig. 5c). The first evolution period involving protons ($t_1^{max} = 1.2$ ms, 32 increments) is implemented only in the 3D experiment to identify the proton spins from which magnetization originates. For the 2D experiments, a spin-temperature filter ensures that magnetization originates from protons, using $\varphi_1 = +x, -x$; $\varphi_2 = 2(-x), 2(+x)$; $\varphi_3 = 4(+x), 4(-x)$; $\varphi_4 = +x$; $\varphi_5 = 8(+y), 8(-y)$; $\varphi_6 = +x$; $\varphi_{REC} = (+x, -x, -x, +x), 2(-x, +x, +x, -x), (+x, -x, -x, +x)$. Scalar decoupling is achieved by a 180° $^{15}N$ pulse in the middle of the evolution period. The heteronuclear NOE mixing time is set to 500 ms. Subsequently, $^{15}N$ chemical shifts are evolved ($t_2^{max} = 3.9$ ms, 16 increments). States-TPPI was used in both indirect dimensions to achieve sign discrimination of the frequency in the rotating frame. A refocused INEPT step is employed to transfer magnetization from $^{15}N$ to $^1H$ (using an optimized effective $J$ coupling of 88 and 92.5 Hz for $^1H$-$^{15}N$ and $^{15}N$-$^1H$ steps, respectively). During acquisition, proton magnetization is acquired (aq = 50 ms) using GARP for $^{15}N$ heteronuclear scalar decoupling. 512 scans are accumulated for each increment. The recycle delay was set to 1.6 s, resulting in a total aquisition time of approximately 5 days.

All MAS solid-state NMR experiments were performed at a magnetic field strength of 9.4 T, employing a Bruker Avance 400WB spectrometer. The spectrometer was equipped with a standard 3.2 mm triple resonance MAS probe. The MAS rotation frequency was set to 20 kHz in all experiments. The effective temperature was adjusted to 30 °C. The $^1H$, $^{13}C$ and $^{15}N$ $\pi/2$ pulse widths used in the $[^1H]^{15}N$ heteronuclear NOE correlation spectra were set to 3.5, 4.2 and 4.5 μs, corresponding to a RF field of 71, 59 and 56 kHz, respectively. WALTZ-16 decoupling was applied on the $^{15}N$ channel ($\omega_{rf}/2\pi = 2$ kHz) during proton acquisition. The recycle delay was set to 3 s. The MISSISSIPI scheme (Zhou and Rienstra 2008) for $^1H$ water dephasing was applied without use of homospoil gradients. All hetNOE spectra are processed by employing cosine squared window functions in both dimensions for apodization, without any resolution enhancement.

## MD simulations

MD simulations were started from the crystal structure of the alpha-spectrin SH3 domain (PDB code: 2NUZ). The 4 SH3 monomers of the asymmetric crystal unit were simulated in an orthorhombic crystal lattice using periodic boundary conditions with cell dimensions 34 × 43 × 50 Å. Simulations were carried out using the Amber99SB all-atom force field in GROMACS 4.5.4 (Hess et al. 2008) with TIP3P water. The simulation system was comprised of 8 unit cells (2 × 2 × 2) containing together 63,437 atoms, including 33,705 solvent molecules, and 114 $Na^+$ ions and 146 $Cl^-$ ions to achieve a salt concentration of 150 mM and thus neutral net charge. LINCS (Hess 2008) and Settle (Miyamoto and Kollman 1992) were applied to constrain covalent bond lengths, allowing an integration time step of 2 fs. Electrostatic interactions were calculated with the particle-mesh Ewald method (Essman et al. 1995). The temperature was kept at a constant 300 K by separately coupling ($\tau = 1$ ps) the peptide and solvent to an external temperature bath using velocity-rescaling (Bussi et al. 2007). The pressure was kept constant by Berendsen coupling ($\tau = 0.5$ ps) to a pressure bath. The simulation was relaxed using steepest-descent followed by a 500 ps equilibration using position restraints on heavy atoms. After the equilibration phase, the simulation was within 0.2 % of the experimentally observed unit cell volume. An NTP simulation was run for 1 μs. Since 32 equivalent SH3 subunits are present in the simulation system, this yields the equivalent of 32 μs of simulation time for a single SH3 subunit.

**Acknowledgments** This research was supported by the Helmholtz-Gemeinschaft, the Leibniz-Gemeinschaft and the DFG (Re1435, SFB1035). We are grateful to the Center for Integrated Protein Science Munich (CIPS-M) for financial support.

## References

Agarwal V, Reif B (2008) Residual methyl protonation in perdeuterated proteins for multidimensional correlation experiments in MAS solid-state NMR spectroscopy. J Magn Reson 194:16–24

Agarwal V, Xue Y, Reif B, Skrynnikov NR (2008) Protein side-chain dynamics as observed by solution- and solid-state NMR: a similarity revealed. J Am Chem Soc 130:16611–16621

Akbey Ü, Lange S, Franks TW, Linser R, Diehl A, van Rossum BJ, Reif B, Oschkinat H (2010) Optimum levels of exchangeable protons in perdeuterated proteins for proton detection in MAS solid-state NMR spectroscopy. J Biomol NMR 46:67–73

Asami S, Reif B (2013) Proton-detected solid-state NMR at aliphatic sites: applications to crystalline systems. Acc Chem Res 46:2089–2097

Asami S, Schmieder P, Reif B (2010) High resolution 1H-detected solid-state NMR spectroscopy of protein aliphatic resonances: access to tertiary structure information. J Am Chem Soc 132:15133–15135

Asami S, Szekely K, Schanda P, Meier BH, Reif B (2012) Optimal degree of protonation for 1H detection of aliphatic sites in randomly deuterated proteins as a function of the MAS frequency. J Biomol NMR 54:155–168

Bussi G, Donadio D, Parrinello M (2007) Canonical sampling through velocity rescaling. J Chem Phys 126:014101

Byeon I-JL, Hou G, Han Y, Suiter CL, Ahn J, Jung J, Byeon C-H, Gronenborn AM, Polenova T (2012) Motions on the millisecond time scale and multiple conformations of HIV-1 capsid protein: implications for structural polymorphism of CA assemblies. J Am Chem Soc 134:6455–6466

Cavanagh J, Fairbrother WJ, Palmer AG, Skelton NJ (1996) Protein NMR spectroscopy: principles and practice. Academic Press, San Diego

Chevelkov V, Faelber K, Diehl A, Heinemann U, Oschkinat H, Reif B (2005) Detection of dynamic water molecules in a microcrystalline sample of the SH3 domain of alpha-spectrin by MAS solid-state NMR. J Biomol NMR 31:295–310

Chevelkov V, Rehbein K, Diehl A, Reif B (2006) Ultra-high resolution in proton solid-state NMR at high levels of deuteration. Angew Chem Int Ed 45:3878–3881

Chevelkov V, Diehl A, Reif B (2007a) Quantitative measurement of differential $^{15}$N-H$\alpha/\beta$ $T_2$ relaxation times in a perdeuterated protein by MAS solid-state NMR spectroscopy. Magn Reson Chem 45:S156–S160

Chevelkov V, Faelber K, Schrey A, Rehbein K, Diehl A, Reif B (2007b) Differential line broadening in MAS solid-state NMR due to dynamic interference. J Am Chem Soc 129:10195–10200

Chevelkov V, Diehl A, Reif B (2008) Measurement of $^{15}$N-$T_1$ relaxation rates in a perdeuterated protein by MAS solid-state NMR spectroscopy. J Chem Phys 128:052316

Chevelkov V, Fink U, Reif B (2009a) Accurate determination of order parameters from $^{1}$H,$^{15}$N dipolar couplings in MAS solid-state NMR EXPERIMENTS. J Am Chem Soc 131:14018–14022

Chevelkov V, Fink U, Reif B (2009b) Quantitative analysis of backbone motion in proteins using MAS solid-state NMR spectroscopy. J Biomol NMR 45:197–206

Chevelkov V, Xue Y, Linser R, Skrynnikov NR, Reif B (2010) Comparison of solid-state dipolar couplings and solution relaxation data provides insight into protein backbone dynamics. J Am Chem Soc 132:5015–5017

Clore GM, Szabo A, Bax A, Kay LE, Driscoll PC, Gronenborn AM (1990) Deviations from the simple 2-parameter model-free approach to the interpretation of N-15 nuclear magnetic relaxation of proteins. J Am Chem Soc 112:4989–4991

Cole HBR, Torchia DA (1991) An NMR-study of the backbone dynamics of staphylococcal nuclease in the crystalline state. Chem Phys 158:271–281

Essman U, Perela L, Berkowitz ML, Darden T, Lee H, Pedersen LG (1995) A smooth particle mesh Ewald method. J Chem Phys 103:8577–8592

Fry EA, Sengupta S, Phan VC, Kuang S, Zilm KW (2011) CSA-enabled spin diffusion leads to MAS rate-dependent T-1's at high field. J Am Chem Soc 133:1156–1158

Gibby MG, Waugh JS, Pines A (1972) Anisotropic nuclear spin relaxation of C-13 in solid benzene. Chem Phys Lett 16:296–299

Giraud N, Böckmann A, Lesage A, Penin F, Blackledge M, Emsley L (2004) Site-specific backbone dynamics from a crystalline protein by solid-state NMR spectroscopy. J Am Chem Soc 126:11422–11423

Giraud N, Sein J, Pintacuda G, Böckmann A, Lesage A, Blackledge M, Emsley L (2006) Observation of heteronuclear Overhauser effects confirms the 15N-1H dipolar relaxation mechanism in a crystalline protein. J Am Chem Soc 128:12398–12399

Helmus JJ, Surewicz K, Nadaud PS, Surewicz WK, Jaroniec CP (2008) Molecular conformation and dynamics of the Y145Stop variant of human prion protein in amyloid fibrils. Proc Natl Acad Sci USA 105:6284–6289

Hess B (2008) P-LINCS: a parallel linear constraint solver for molecular simulation. J Chem Theory Comput 4:116–122

Hess B, Kutzner C, van der Spoel D, Lindahl E (2008) GROMACS 4: algorithms for highly efficient, load-balanced, and scalable molecular simulation. J Chem Theory Comput 4:435–447

Higgins JS, Hodgson AH, Law RV (2002) Heteronuclear NOE in the solid state. J Mol Struct 602:505–510

Hou G, Byeon I-JL, Ahn J, Gronenborn AM, Polenova T (2011) H-1-C-13/H-1-N-15 heteronuclear dipolar recoupling by R-symmetry sequences under fast magic angle spinning for dynamics analysis of biological and organic solids. J Am Chem Soc 133:18646–18655

Ishima R, Louis JM, Torchia DA (2001a) Optimized labeling of $^{13}CHD_2$ methyl isotopomers in perdeuterated proteins: potential advantages for $^{13}$C relaxation studies of methyl dynamics of larger proteins. J Biomol NMR 21:167–171

Ishima R, Petkova AP, Louis JM, Torchia DA (2001b) Comparison of methyl rotation axis order parameters derived from model-free analyses of H-2 and C-13 longitudinal and transverse relaxation rates measured in the same protein sample. J Am Chem Soc 125:6164–6171

Katoh E, Takegoshi K, Terao T (2004) C-13 nuclear overhauser polarization-magic-angle spinning nuclear magnetic resonance spectroscopy in uniformly C-13-labeled solid proteins. J Am Chem Soc 126:3653–3657

Knight MJ, Webber AL, Pell AJ, Guerry P, Barbet-Massin E, Bertini I, Felli IC, Gonnelli L, Pierattelli R, Emsley L, Lesage A, Herrmann T, Pintacuda G (2011) Fast resonance assignment and fold determination of human superoxide dismutase by high-resolution proton-detected solid-state MAS NMR spectroscopy. Angew Chem Int Ed 50:11697–11701

Knight MJ, Pell AJ, Bertini I, Felli IC, Gonnelli L, Pierattelli R, Herrmann T, Emsley L, Pintacuda G (2012) Structure and backbone dynamics of a microcrystalline metalloprotein by solid-state NMR. Proc Natl Acad Sci USA 109:11095–11100

Krushelnitsky A, Zinkevich T, Reichert D, Chevelkov V, Reif B (2010) Microsecond time scale mobility in a solid protein as

studied by the N-15 R-1 rho site-specific NMR relaxation rates. J Am Chem Soc 132:11850–11853

Lewandowski JR, Dumez JN, Akbey U, Lange S, Emsley L, Oschkinat H (2011a) Enhanced resolution and coherence lifetimes in the solid-state NMR spectroscopy of perdeuterated proteins under ultrafast magic-angle spinning. J Phys Chem Lett 2:2205–2211

Lewandowski JR, Sass HJ, Grzesiek S, Blackledge M, Emsley L (2011b) Site-specific measurement of slow motions in proteins. J Am Chem Soc 133:16762–16765

Linser R, Chevelkov V, Diehl A, Reif B (2007) Sensitivity enhancement using paramagnetic relaxation in MAS solid state NMR of perdeuterated proteins. J Magn Reson 189:209–216

Linser R, Fink U, Reif B (2009) Probing surface accessibility of proteins using paramagnetic relaxation in solid-state NMR spectroscopy. J Am Chem Soc 131:13703–13708

Linser R, Fink U, Reif B (2010) Detection of dynamic regions in biological solids enabled by spin-state selective NMR experiments. J Am Chem Soc 132:8891–8893

Lopez del Amo J-M, Fink U, Reif B (2010) Quantification of protein backbone hydrogen–deuterium exchange rates by MAS solid-state NMR spectroscopy. J Biomol NMR 48:203–212

Lorieau JL, McDermott AE (2006) Conformational flexibility of a microcrystalline globular protein: order parameters by solid-state NMR spectroscopy. J Am Chem Soc 128:11505–11512

Miyamoto S, Kollman PA (1992) SETTLE: an analytical version of the SHAKE and RATTLE algorithms for rigid water models. J Comput Chem 13:952–962

Purusottam RN, Bodenhausen G, Tekely P (2013) Quantitative one- and two-dimensional C-13 spectra of microcrystalline proteins with enhanced intensity. J Biomol NMR 57:11–19

Quinn CM, McDermott AE (2012) Quantifying conformational dynamics using solid-state R-1 rho experiments. J Magn Reson 222:1–7

Schanda P, Huber M, Verel R, Ernst M, Meier BH (2009) Direct detection of 3hJNC hydrogen-bond scalar couplings in proteins by solid-state NMR spectroscopy. Angew Chem Int Ed 48:9322–9325

Schanda P, Meier BH, Ernst M (2010) Quantitative analysis of protein backbone dynamics in microcrystalline ubiquitin by solid-state NMR spectroscopy. J Am Chem Soc 132:15957–15967

Schanda P, Meier BH, Ernst M (2011) Accurate measurement of one-bond H–X heteronuclear dipolar couplings in MAS solid-state NMR. J Magn Reson 210:246–259

Skrynnikov NR, Millet O, Kay LE (2002) Deuterium spin probes of side-chain dynamics in proteins. 2. Spectral density mapping and identification of nanosecond time-scale side-chain motions. J Am Chem Soc 124:6449–6460

Takegoshi K, Terao T (2002) C-13 nuclear Overhauser polarization nuclear magnetic resonance in rotating solids: replacement of cross polarization in uniformly C-13 labeled molecules with methyl groups. J Chem Phys 117:1700–1707

Tollinger M, Sivertsen AC, Meier BH, Ernst M, Schanda P (2012) Site-resolved measurement of microsecond-to-millisecond conformational-exchange processes in proteins by solid-state NMR spectroscopy. J Am Chem Soc 134:14800–14807

White JL, Haw JF (1990) Nuclear overhauser effect in solids. J Am Chem Soc 112:5896–5898

Wylie BJ, Franks T, Graesser DT, Rienstra CM (2005) Site-specific C-13 chemical shift anisotropy measurements in a uniformly N-15, C-13-labeled microcrystalline protein by 3D magic-angle spinning NMR spectroscopy. J Am Chem Soc 127:11946–11947

Xue Y, Pavlova MS, Ryabov YE, Reif B, Skrynnikov NR (2007) Methyl rotation barriers in proteins from 2H relaxation data. Implications for protein structure. J Am Chem Soc 129:6827–6838

Zhou DH, Rienstra CM (2008) High-performance solvent suppression for proton-detected solid-state NMR. J Magn Reson 192:167–172

Zinkevich T, Chevelkov V, Reif B, Saalwachter K, Krushelnitsky A (2013) Internal protein dynamics on ps to μs timescales as studied by multi-frequency 15N solid-state NMR relaxation. J Biomol NMR 57:219–235